PCCP

Cite this: *Phys. Chem. Chem. Phys.*, 2012, **14**, 10595–10602

www.rsc.org/pccp

PAPER

Morphology and crystallization kinetics of compact (HGW) and porous (ASW) amorphous water ice

Belén Maté,* Yamilet Rodríguez-Lazcano and Victor J. Herrero

Received 23rd March 2012, Accepted 11th June 2012
DOI: 10.1039/c2cp41597f

An investigation of porosity and isothermal crystallization kinetics of amorphous ice produced either by background water vapour deposition (ASW) or by hyperquenching of liquid droplets (HGW) is presented. These two types of ice are relevant for astronomical ice research (Gálvez *et al.*, *Astrophys. J.*, 2010, **724**, 539) and are studied here for the first time under comparable experimental conditions. From CH_4 isothermal adsorption experiments at 40 K, surface areas of 280 ± 30 $m^2\ g^{-1}$ for the ASW deposits and of 40 ± 12 $m^2\ g^{-1}$ for comparable HGW samples were obtained. The crystallization kinetics was studied at 150 K by following the evolution of the band shape of the OD stretching vibration in HDO doped ASW and HGW samples generated at 14 K, 40 K and 90 K. Comparable rate constants of $\sim 7 \times 10^{-4}\ s^{-1}$ were obtained in all cases. However a significant difference was found between the *n* Avrami parameter of the samples generated at 14 K ($n \sim 1$) and that of the rest ($n > 2$). This result hints at the possible existence of a structurally different form of amorphous ice for very low generation temperatures, already suggested in previous literature works.

Introduction

Water ice, with different morphologies and structures, is not restricted to the Earth but is also found on many solid bodies in the Solar System and on the surface of dust grains in interstellar space. Non-crystalline solid water is metastable with respect to its crystalline phase, the common form of ice found on our planet.[1,2] Since "amorphousness" is hard to quantify, the different forms of amorphous ice are usually distinguished by the method of preparation or by the sample history.

Amorphous ice was generated by vapour deposition on a cold substrate as early as 1935.[3] This generation procedure leads to a microporous solid,[4,5] which is usually termed amorphous solid water (ASW). X-ray and electron diffraction experiments[6–9] pointed to the existence of two forms of ASW differing in their intrinsic density (*i.e.* the density excluding pore volume). According to these works, vapour deposition at very low temperatures ($T \approx 10$ K) leads to a high density ($\rho = 1.1\ g\ cm^{-3}$) phase, whereas deposition at temperatures higher than ~30 K produces the more common low density ($\rho = 0.94\ g\ cm^{-3}$) form. However, the existence of the high-density ASW phase has been contested in the literature (see for instance ref. 10 and the discussion in ref. 4). Beyond ~125 K ASW crystallizes into cubic ice (I_c). Although irreversible transitions between the mentioned ice phases occur with increasing temperature, complete phase transformation within a given ice sample is usually slow on laboratory time-scales and phase mixtures are often observed. High- and low-density ASW, and also amorphous and crystalline domains have been reported to co-exist over a temperature range.[7,11] Besides temperature, deposition rate was found to appreciably influence the degree of disorder of the ice;[12–15] in general, a higher deposition rate leads to more disordered samples. Essentially amorphous ice was obtained by Mitling and Leung[16] through vapour deposition at a temperature as high as 145 K with a growth rate of 1.5 μm h^{-1}.

In a recent paper, dealing mostly with comparatively high temperature and pressure samples, Loerting *et al.*[17] argued that true polyamorphic "states" of ice could be reduced to just three: low (LDA), high (HAD) and very high density (VHDA), and that the large variety of amorphous samples that can be obtained experimentally would correspond to "substates" of one of these three forms. However, the physical and chemical properties of amorphous ice do not depend only on its molecular structure, but are also closely related to its bulk morphology, a characteristic also strongly affected by the generation conditions.[4,5,17]

In this work we will concentrate on two forms of amorphous ice, the already mentioned ASW and "hyperquenched glassy water" (HGW) which is formed by rapid cooling of liquid water droplets.[18,19] Both ASW and HGW might be relevant in laboratory studies of astronomical ice analogues (see below). X-ray and neutron-diffraction measurements have shown that at ~80 K, the two forms have the same intrinsic density (0.94 g cm^{-3}) and also similar atomic-level structures[20,21] and, therefore, they

Instituto de Estructura de la Materia, IEM-CSIC, Serrano 121-123, 28006, Madrid, Spain. E-mail: belen.mate@csic.es

would both correspond to forms of LDA in the classification of Loerting *et al.*[17] We are not aware of comparative structural studies of ASW and HGW at lower temperatures.

It is expected that the two forms of ice under consideration present very different micro- and mesoscale morphologies with ASW being variously porous and HGW being compact. The porosity of ASW depends dramatically on the details of its production. Under suitable generation conditions, bulk densities as low as 0.2 g cm^{-3} have been measured for some ASW samples.[22–24] Such differences were explained by an increase in the porosity with the angle of incidence of the water molecules impinging on the substrate. Although the intrinsic density of the ice still is 0.94 g cm^{-3}, the bulk density decreases when the voids are taken into account. Other experimental conditions like deposition rate, the composition and pressure of the background gas during deposition, or the presence of a carrier gas, which could be deposited simultaneously with the water vapour, affect also the porosity of the ice.

Annealing of ASW below the crystallization temperature may induce a substantial collapse of the pores and thus a compaction of the ASW sample (see for instance[4,24,25] and references therein). As in the case of phase transformations commented on above, pore collapse upon annealing takes a long time to complete on laboratory time scales[26] and there are indications that some internal pores and cavities persist until crystallization.[27,28] In any case it is not obvious *a priori* that the compact ice morphology of annealed ASW is entirely equivalent to that of HGW.

The morphology of the ices can be characterized with different experimental methods. The measurement of the index of refraction by interferometric techniques allows the determination of the density and the derivation of a porosity factor.[29,30] OH-dangling bond absorptions present in the infrared spectra of the ices are associated with uncoordinated water molecules at ice surfaces and also provide information on the amount of pores in the solid.[31–33] Isothermal adsorption of gases is a broadly used technique to characterize the porosity of a solid that allows the estimation of specific surface areas and pore sizes, and has been widely applied to water ice.[34,35] Extensive studies on the amorphous solid water porosity have been conducted over the last decades, but a broad dispersion of results was found, which, as already mentioned, might be motivated by the varied generation conditions of the ice deposits. For example, the reported specific surface area of ASW at 77 K ranged from 3 m^2 g^{-1} to 400 m^2 g^{-1}.[36–40] Very different results were also measured for the OH-dangling bond/OH-stretching band intensity ratio in the IR spectra of different ASW ices.[24,25,32,41–43]

Metastable amorphous ice samples will eventually crystallize when heated to a high enough temperature for a sufficiently long time period. The crystallization kinetics of amorphous ices has been studied using a variety of techniques, including temperature programmed desorption (TPD) and infrared spectroscopy (see ref. 44 and references therein). Crystallization is observed to occur between 140 K and 170 K, and the crystallization rate depends on experimental parameters like ice generation conditions, heating ramp or thickness of the sample.[28,44–46]

From an astrophysical point of view the study of amorphous solid water is highly interesting since it is generally assumed that most of the water in the universe is locked in the form of amorphous ice on dust grains in dense interstellar clouds, and on cold bodies in planetary systems. In those objects ice can adopt varied structures and morphologies depending on their history and particular properties.[4,5,47] Low temperature (<20 K) deposition of water molecules from the vapour phase on the grains of molecular clouds is expected to lead to a microporous morphology presumably similar to that of ASW.[4] Ice analogous to HGW may be formed on the surface of icy satellites or on outer solar system bodies when water, liquefied after the impact of a meteorite, freezes almost instantly,[5] and more generally, compact ice can form on grain surfaces through reactions of adsorbed species.[48,49] Laboratory experiments have shown that porous ices can also be compacted through interaction with high energy ions[50,51] in a process similar to that expected for cosmic ray bombardment. Astronomical ices, which are usually observed through their mid-IR spectra, are always dominated by water, but many other molecules (CO, CO_2, NH_3...) are also found in appreciable amounts and even some ions (OCN^-, NH_4^+, $HCOO^-$) have been tentatively identified as minor constituents.[52] Recent laboratory work by our group led to the production of ASW and HGW samples including NH_4^+ and $HCOO^-$ ions.[53,54] It is worth noting that the hyperquenching technique provides a very convenient way of introducing a known chemical species, in particular ions, into a compact ice network. Large differences were observed in the IR intensities of the ions in the two ice matrices, with HGW samples leading to much weaker ion band intensities. The results strongly suggested that the NH_4^+ ion, tentatively assigned in the literature as the carrier of the IR 6.85 μm band found in many interstellar ice spectra, should be virtually undetectable when embedded in the compact HGW ice.

In this work we present a joint investigation of the two types of laboratory ices, ASW and HGW, commented on thus far in order to establish differences and similarities in their morphology and crystallization behaviour. The pertinence of this comparative study should be stressed here because the large dispersion of data available in the literature is often confusing and it is important to guarantee that the ice samples are investigated under comparable conditions. We are not aware of a similar previous study on these amorphous ice varieties relevant for astronomical research.

The ices were generated at 14 K, 40 K and 90 K by background vapour deposition (ASW) or by hyperquenching of liquid water droplets (HGW). We have analyzed the variations in the IR spectra of both forms of ice. Their specific surface area was measured *via* isothermal adsorption of methane at 40 K. We have also conducted crystallization kinetics experiments, determining their crystallization rate constants at 150 K *via* the Avrami model.[55] We expect that these studies mimicking astrophysical ices with different morphologies will help us to understand the chemistry that may take place on them, and therefore can be of help for the interpretation of astronomical observations.

Experimental part

The experiments were conducted in a high vacuum chamber, with a base pressure of 1×10^{-8} mbar. A more detailed description of our experimental setup was given in previous papers.[56,57] The deposition substrate is a mid-infrared transparent Si plate in close contact with a closed-cycle He cryostat.

The sample temperature was controlled between 14 K and room temperature with 1 K accuracy by means of a heating foil. Distilled water was used in all the experiments. The main chamber is coupled, by means of a regulation valve, to a differentially pumped chamber containing an Inficon Transpector 2 quadrupole mass spectrometer (QMS), which is used to monitor the purity and stability of the vapour during the deposition process. Infrared transmission spectra in the 4000–500 cm^{-1} range were obtained with a Vertex70 Bruker FTIR spectrometer coupled to the vacuum chamber through a purged pathway. The infrared beam exiting the chamber was focused onto a liquid nitrogen cooled mercury cadmium telluride (MCT) detector. Infrared spectra with a resolution of 2 cm^{-1} were averaged for 300 scans.

The amorphous ice samples were grown using two different techniques: (a) by introducing water vapour in the vacuum chamber through a leak valve, *i.e.*, by background deposition (amorphous solid water, ASW), and (b) by injecting a directed flow of liquid water droplets perpendicular to the substrate (hyperquenched glassy water,[18] HGW). The droplets were expelled from a room temperature pulsed valve (General Valve, series 9), usually employed for the generation of free jets and molecular beams.[58] The exit orifice has a 0.5 mm nominal diameter and the distance between the valve exit and the substrate was ~10 mm. The deposition time for HGW deposits was very short, usually one or two valve pulses of 5 ms. In these experiments the substrate was rotated under vacuum to situate its surface perpendicular to the nozzle flow and the water droplets from the valve reached just one face of the substrate. Once the ice deposit was formed, the substrate was rotated back to its original position for recording the transmission spectra. In a separate experiment we have visualized the shape of the deposits and have found that they consist of an irregular central region, containing most of the ice, formed by piled up frozen droplets, and of individual or small groups of frozen droplets scattered through the rest of the substrate surface. We estimate that the HGW deposits cover roughly half the substrate face where they impinge. To grow a vapour deposited ASW solid with a similar number of molecules took between 15 and 20 min. The chamber was backfilled with a water pressure of $\sim 1.5 \times 10^{-5}$ mbar and infrared spectra were recorded during the deposition process until the intensity of the OH-stretching absorption band matched that of the HGW deposit of interest. During the deposition process vapour composition was monitored with a quadrupole mass spectrometer. The N_2 impurity was always below 0.1% and this low level should not have affected the morphology of the ice deposited at 14 K.

The morphology (porosity) of the ASW and HGW films was probed both by comparing their IR absorption bands, and by monitoring CH_4 uptake in the two types of samples. In the ASW experiment, the deposition took place directly on both sides of the IR transparent substrate. During the cooling of the substrate to 14 K a thin layer of ASW is grown on both sides due to background water vapour. In the HGW experiments a correction was introduced to account for CH_4 uptake on the thin ASW film not covered by the HGW deposits. This correction amounted to about 20% of the adsorbed methane.

In the CH_4 uptake experiments, after generating an ice film at 40 K the chamber was backfilled with a CH_4 pressure by means of a needle valve, and spectra were recorded continuously. The methane pressure was increased smoothly from an initial value of 2×10^{-7} mbar to the saturation pressure, defined as the lowest pressure were multilayers of solid methane start to grow. In our experiments it was found to be 6.9×10^{-6} mbar. The CH_4 uptake on the surface of the ice was monitored by following the evolution of the ν_4 band of methane at ~7.7 μm (1300 cm^{-1}).

Absolute water (or methane) pressures were determined from the growing rates of background deposited films of pure H_2O (or CH_4). Film thickness values, necessary for the growing rate estimations, can be derived from the IR spectra *via* the Lambert–Beer relation. The integrated band strength of the OH-stretching of water was chosen for this purpose and we take the values of $A = 1.9 \times 10^{-16}$ cm per molecule, 2.1×10^{-16} cm per molecule and 3.0×10^{-16} cm per molecule for vapour deposited ice at 15 K, 40 K and 100 K, respectively.[59] For the ν_4 band of CH_4 an integrated band strength of $A = 8.085 \times 10^{-18}$ cm per molecule was taken from Hudgins *et al.*[60] (corrected for a CH_4 density[61] of 0.47 g cm^{-3}). From the growing rate we determine the absolute pressure and calibrate the QMS for the masses 18 and 16, as reported in a previous work.[56]

In the crystallization kinetics experiments HGW and ASW samples, with a small HDO admixture, were prepared at 14 K, 40 K, or 90 K. The samples were annealed at 5 K min^{-1} to 150 K and the evolution of the ice at this temperature was monitored *via* infrared spectroscopy of the OD band of HDO. Changes in the shape of this band upon crystallization are easier to identify than in the much broader OH band of the ice.[45] Spectra were recorded at short time intervals (1 or 3 min) over 1 h. In all cases the evolution was finished before this time.

Results and discussion

The dangling bond bands

Fig. 1 shows infrared absorption spectra in the region of the OH stretching band of the two forms of amorphous ice investigated in this work. The condensed phases of H_2O are characterized by the presence of 4-coordinated hydrogen bonded units. There is also a small amount of water molecules with an H-atom that is not involved in hydrogen bonding. These bonds are referred to as dangling-bonds (DB) and give rise to the DB band. At 14 K two kind of DB bands are present, evidenced by a doublet at 3720 cm^{-1} and 3696 cm^{-1} that correspond, respectively, to doubly- and triply-coordinated surface water molecules.[62] A sketch of the incomplete coordination of H_2O molecules at the surface of the ice can be found in Fig. 1 of ref. 62. The DB bands have been represented enlarged in panels c and d of Fig. 1. These bands are related to the surface area and thus to the porosity of the sample.[63,64] The DB band area in the spectrum of the ASW film grown at 14 K (panels a and c, black trace) represents 0.04% of the OH-stretching band total intensity. When the ASW is deposited at 40 K the DB/OH-stretching band intensity ratio decreases by a factor ~1.5 (see panel d), representing only 0.026% of the OH stretching total intensity, and in this case the weaker component associated with doubly-coordinated surface molecules has practically vanished.

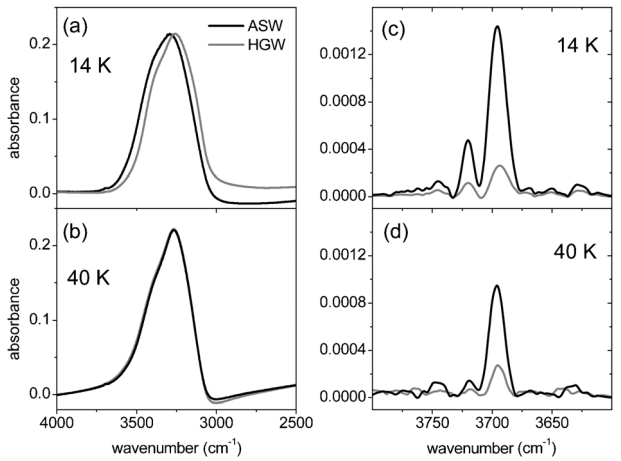

Fig. 1 Infrared spectra of the OH stretching region of ASW (black) and HGW (grey) ices ~100 nm thick generated at 14 K (panel a) and 40 K (panel b). Panels (c) and (d): an enlargement of the dangling-bond spectral region of the spectra presented in panels (a) and (b), respectively.

This behaviour indicates that the ice grown at 40 K is less porous. The preferential reduction in the amount of 2-coordinated surface molecules was already observed by Kimmel *et al.*[35] They mentioned that the number of 3-coordinated molecules was almost unaltered when ices grown at 22 K were annealed to 65 K. However, in that same paper, the authors conclude that the porosity of the samples decreases with the temperature of generation, as measured by a decrease in the N_2 gas uptake. In our experiments, the ices grown at 90 K do not show any DB bands. For HGW generated at 14 K or 40 K the DB band (grey trace) is about seven times smaller than its ASW counterpart, which illustrates the appreciably lower surface (*i.e.* higher compactness) of the HGW sample.

We have tried to compare the intensity of the DB band with other results in the literature. In the amorphous ice grown at 40 K by Raut *et al.*[33] by background deposition, the DB band represents approximately 0.1% of the OH-stretching band, which is close to our value, indicating analogous morphology as expected due to the very similar generation conditions. However, it is well known that reflection–absorption (RAIR) spectra, as those presented in ref. 33, are prone to possible intensity distortions inherent to this technique, which puts a word of caution on a comparison with our transmission spectra. In particular, and in contrast to IR transmission spectra, the RAIR band intensities are no longer proportional to the ice film thickness, as highlighted in a previous work by our group.[56] Other IR spectra of amorphous ices generated in various ways (co-deposited with other volatiles[40,43] or with molecular beams at large incident angles)[24] display DB bands orders of magnitude stronger than those observed in our work, pointing to a much higher porosity of these samples.

The specific surface area

Adsorption isotherms of CH_4 on amorphous ASW and HGW ices are presented in Fig. 2. Various weak interacting molecules are usually chosen for these types of studies. Kimmel *et al.*[35] showed, for instance, that the use of N_2, Ar and CH_4 to characterize the porosity of ASW films led to reasonably similar results. In our case the choice of methane as a probe molecule is dictated by experimental convenience, since the study is based on IR spectroscopy and CH_4 has IR active bands. The weak interaction of CH_4 with water molecules in the ice leads to small distortions of the molecule, which are manifest as small frequency shifts in the CH_4 spectral features (see ref. 65 and 66 for a thorough discussion). These weak interactions hardly affect the intense ν_4 band, which is the one relevant for the present measurements. Samples of the two types of ice with a similar number of water molecules were prepared by comparing the OH-stretching band intensity in their infrared spectra. The ices were grown at 40 K, to avoid the formation of CH_4 multilayers at low methane pressures. This temperature is well below the triple point of methane that occurs at about 90 K. The figure shows the proportion of gas molecules adsorbed on the surface of the ice (expressed as n_{CH_4}/n_{H_2O} molecular ratios) plotted *versus* the equilibrium methane pressure normalized by the corresponding saturation pressure, p_0. This saturation pressure corresponds to the sublimation pressure of solid methane at 40 K. The molecular ratio was obtained from the ratio of the intensities of the 1300 cm^{-1} band of methane to the 3200 cm^{-1} band of water. The amount of methane adsorbed on ASW is ~5.3 times larger than that on HGW for deposits having the same number of H_2O molecules.

We applied the Brunnauer, Emmet and Teller (BET) model[67] to determine the specific surface area, SSA, of our amorphous ices. Two parameters can be determined by fitting the linear transformed BET equation, the monolayer capacity ν_m, and the constant c:

$$\frac{p}{\nu(p-p_0)} = \frac{1}{\nu_m c} + \frac{c-1}{\nu_m c}\frac{p}{p_0}$$

Here ν is the amount of gas absorbed on the surface. The SSA is derived from the monolayer coverage, ν_m, assuming the methane molecules have an effective mean area of 14.8 $Å^2$. The c parameter provides information about the net heat of adsorption that represents the difference between the adsorption energy and the condensation energy. It is related to the net heat of absorption ΔQ by the expression: $\Delta Q = kT\ln c$.

The specific surface areas extracted from the fits of the data of Fig. 2 to the BET model are 280 ± 30 $m^2\ g^{-1}$ and 40 ± 12 $m^2\ g^{-1}$

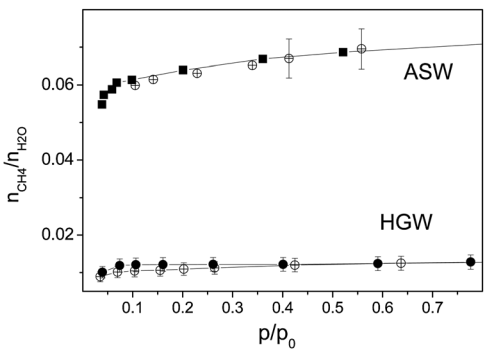

Fig. 2 CH_4 uptake molecular ratio *versus* methane pressure, normalized by the saturation pressure, for ice films ~100 nm thick grown at 40 K by vapour deposition (ASW) or hyperquenching (HGW).

for ASW and HGW, respectively. We have estimated the uncertainty from the dispersion on the different isotherm absorption experiments. We have a ±8% error in the experimental isotherm data for vapour deposited ices and a 15% error for the hyperquenched ones, where the reproducibility in the ice generation procedure is somewhat worse.

From these experiments we can conclude that HGW ices are more compact than ASW ices. Intuitively, it can be understood that the sudden freezing of droplets in HGW experiments produces an irregular deposit with a lower surface/volume ratio than the thin film obtained by vapour deposition. The SSA of the compact ice might be mainly due to its external surface. In contrast, in the case of ASW the higher surface area accessible to methane molecules is due to its microporous morphology.[4] Note that the adsorption results are in good accordance with the estimates obtained on inspection of the dangling-bond bands. In both cases, the ASW samples are estimated to have a surface area roughly seven times larger than that of their HGW counterparts.

There is a large dispersion in the literature SSA values for amorphous solid ices. It is nowadays well known that the generation conditions affect the morphology of the ice samples and it is also widely accepted that this is the main reason for the disparity of the literature results. The first studies on the subject were conducted on ices grown at liquid nitrogen temperatures by very fast condensation and without high vacuum conditions: ref. 36 (77 K, 241 $m^2 g^{-1}$), ref. 68 (77 K, 34 $m^2 g^{-1}$), ref. 38 (77 K, 258 $m^2 g^{-1}$), ref. 39 (83 K, 102 $m^2 g^{-1}$). Later on, the experiments were conducted in high vacuum chambers directing water vapour flows to a cold surface: ref. 37 (77 K, 421 $m^2 g^{-1}$), ref. 69 (H_2O : Ar (1 : 30), 56 K, 95–315 $m^2 g^{-1}$). Large surface areas were estimated for high incidence angles and low temperatures: ref. 35 (22 K, 2700 $m^2 g^{-1}$). Our ice samples have been generated at 40 K either by background vapour deposition (280 $m^2 g^{-1}$) or by hyperquenching of liquid droplets (40 $m^2 g^{-1}$). The strong dependence of the SSA on many experimental variables renders difficult a comparison of different literature results if they do not have some common generation conditions, like for example, growth temperature or film thickness. The goal of the present investigation was to compare the SSA of two of the forms of amorphous ice widely studied in laboratories, porous vapour deposited and compact hyperquenched. We have generated ices at the same temperature and have made sure that they contain the same amount of water molecules in order to meaningfully compare their specific surface areas. Our results provide a quantitative estimate of the different compactness of the two types of ice investigated and as far as we know, a similar comparison has not been reported previously in the literature.

Crystallization kinetics

The crystallization kinetics of ASW and HGW has been studied at 150 K following the procedure described by Hage and coworkers.[45] A solution 0.2% in weight of D_2O in H_2O was prepared to generate ices from its vapour (ASW) or by hyperquenching of its droplets (HGW). In this way the ices formed were doped with a small amount of HDO (0.4 wt%). Samples were grown at 14 K, 40 K, and 90 K and subsequently heated at 5 K min^{-1} to 150 K. It is known that a collapse of the microporous structure of vapour deposited water ices takes place in the 80 K–120 K range.[24,25] The transformation at 150 K from an amorphous to a crystalline cubic phase was monitored as a function of time by following the evolution of the OD stretching band with infrared spectroscopy. For this low HOD concentration, OD–OD interactions do not contribute to the bandwidth and the OD stretching transition appears much narrower than the predominant OH stretching.[70] Immediately after reaching 150 K the samples are mainly amorphous and the OD-stretching band takes the shape of a broad peak centred at 2445 cm^{-1}, as can be seen in the top panel of Fig. 3. The band shape changes continuously with time during the process of crystallization, as illustrated in Fig. 3. The initial broad band at 2445 cm^{-1} weakens and a narrower small contribution near 2425 cm^{-1} starts to grow from the first minutes. The broad peak is associated with the stretching vibration of uncoupled OD oscillators surrounded

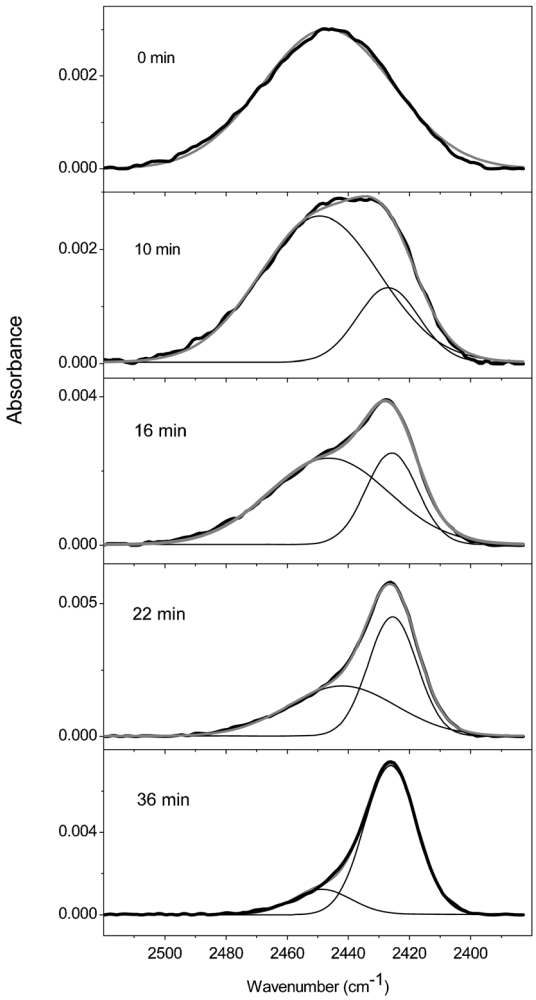

Fig. 3 Infrared spectra of the OD-stretching vibration of HDO in 0.4% HDO doped water ice generated at 40 K by hyperquenching (HGW) and heated at 5 K min^{-1} to 150 K. The time spent by the ice at 150 K is indicated in each panel. The band profiles have been fitted to two Gaussians, with varied widths and fixed peak positions. The integrated areas provide information about the fraction of ice that is in the crystalline form at increasing times.

by an amorphous water environment and the low frequency narrower band is due to OD-oscillators when they are surrounded by water molecules arranged in a crystalline ice form.[71] To follow the crystallization process, the OD band was deconvolved into two Gaussians with almost-fixed peak positions (the peak positions varied 2425 ± 0.5 cm^{-1} for the narrow band and 2445 ± 2 cm^{-1} for the broad one) using a peak fitting routine. When the evolution finished (*i.e.* when no spectral changes were observed in 10 min) the area of the 2425 cm^{-1} band was chosen to represent 100% crystallized ice, a criterion necessary to calculate the fraction of crystallized ice as a function of time. However, in all the experiments it is appreciated that, at the end of the evolution, the OD-band is not completely symmetric, indicating that a small fraction of amorphous phase remains. The presence of an amorphous phase that coexists with cubic crystalline ice when the amorphous samples are heated at 140–160 K has been documented in the literature.[7] We have observed that the fraction on non-crystalline phase remaining at the end of the crystallization process depends on the ice generation temperature and, slightly, on the generation procedure. The values, that have an estimated error of 15%, are displayed in the right column of Table 1. We have found that the higher the generation temperature the smaller the uncrystallised final fraction. The final non-crystalline fraction from compact HGW ices seems to be slightly smaller than that from porous ASW ices (right column of Table 1).

The time evolution of the fraction of ice crystallized at 150 K has been represented *versus* the logarithm of time in Fig. 4, for both ASW and HGW ices grown at 14 K, 40 K and 90 K. Although in all cases the ice evolution finished after 50 min, ices grown at 14 K display a different behaviour, with a slower growth of the fraction of crystallized ice since the first minutes (compare panel a with panels b and c in Fig. 4). The isothermal phase transformation from an amorphous to a crystalline phase can be described by the Avrami equation:[55]

$$x = 1 - \exp(-kt^n)$$

where x is the fraction of crystallized ice, k is a rate coefficient and n is a parameter which depends on growth dimensions and nucleation rate and may have a complicated interpretation. The values of k and n can be derived from a fit of the data presented in Fig. 4 to the Avrami equation expressed in a linear form: $\ln[-\ln(1 - x)] = \ln k + n \ln t$. A typical plot is represented in Fig. 5. In Table 1 are given the n and k values obtained from the fits for all the ices investigated in this work.

The rate coefficients for ices grown at 14 K and 40 K are relatively similar and their mutual variations lie within the (large) experimental error. The rate constants appear somewhat lower for the ices grown at 90 K but do not reflect any clear difference between porous and compact ices. Recent work has highlighted the key role of surface and subsurface dynamics[72,73] in the kinetics of transition between condensed phases (freezing/melting) of H_2O and, in principle, similar surface effects might induce differences in the crystallization of porous and compact ices. In the present case however, the large initial SSA of the 14 K and 40 K ASW is expected to decrease to a great extent as a result of the extensive pore collapse undergone by these ice samples before reaching the temperature (150 K) of the crystallization study. Although the collapse of the pores might not be complete[27,28] the compaction of ASW renders its bulk morphology closer to that of HGW. Even if the morphologies of HGW and annealed ASW are not identical at 150 K, the possible differences do not seem to be too relevant for the crystallization rate coefficients.

In contrast the n parameters, which are determined with a higher accuracy than the rate coefficients, display quite different values, changing between 1 and 2.4 for the two kinds of ice (see Table 1). As indicated above, a high density ASW phase has been previously described in the literature for vapour deposited ices grown on a substrate held at a temperature below 30 K. However, the nature of this ice phase is under debate in the literature.[4,10] The different n values found in the present work for the 14 K ices as compared with those produced at 40 and 90 K, and the closer results in all cases between the ASW

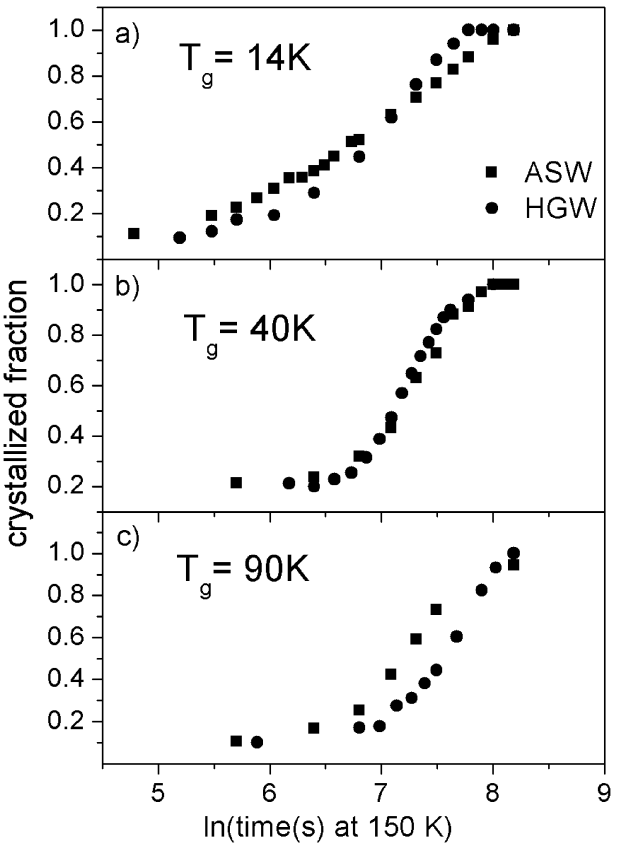

Fig. 4 Fraction of water ice crystallized at 150 K *versus* the logarithm of time at 150 K for ices grown at (a) 14 K, (b) 40 K and (c) 90 K. Closed squares refer to ASW and open circles to HGW.

Table 1 The parameters of crystallization at 150 K of ASW and HGW grown at different temperatures

Generation method	Generation temperature (K)	n	k (10^{-4} s^{-1})	No-cryst fraction (area %)
ASW	14	1.00 ± 0.02	8.8 ± 1.0	22
HGW	14	1.20 ± 0.07	8.3 ± 4.0	20
ASW	40	2.04 ± 0.10	6.6 ± 2.5	15
HGW	40	2.39 ± 0.03	7.0 ± 0.6	14
ASW	90	2.17 ± 0.02	6.3 ± 0.4	13
HGW	90	2.41 ± 0.11	4.7 ± 1.8	11

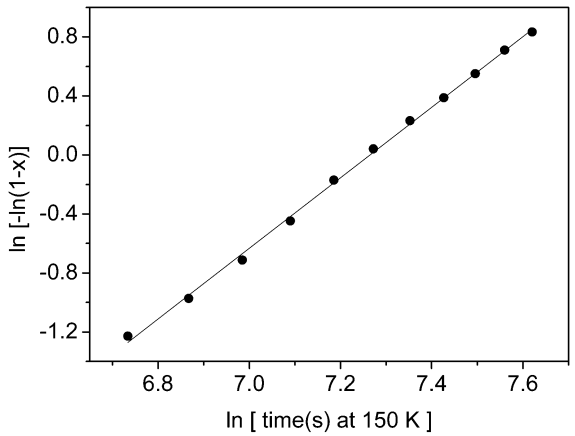

Fig. 5 Avrami linear plot for an HGW ice sample grown at 40 K.

and HGW samples, suggest that a different ice structure, independent from the bulk morphology, might indeed form at very low temperatures ($T < 30$ K). The support provided by the present HGW samples to this hypothesis, which is hitherto essentially based on ASW investigations, should be stressed. Nevertheless, the present experiments based just on IR spectroscopy do not allow a firm statement on this point. Additional experiments employing structurally more resolving diffraction techniques would be needed.

According to the usual interpretation of the Avrami n parameter, the lower n values found for the ices formed at 14 K point to a more restricted dimensionality in their crystallization kinetics as compared with that of the samples generated at 40 K and 90 K. There is also a small but systematic dominance in the n values of HGW over ASW ices, which might reflect an incomplete compaction of ASW upon annealing.

A comparison of our results with those previously reported in the literature is again conditioned by the different generation techniques used to grow the ice films. The ices studied by Hage and coworkers[45] were grown by hyperquenching of water droplets, accompanied by N_2 as the carrier gas, on a cold substrate held at 78 K. They doped the ices with HDO and, using a similar procedure as we did, obtained crystallization rate constants that varied between 1.1×10^{-4} s^{-1} and 1.2×10^{-3} s^{-1}, and n values that ranged between 0.9 and 2.4, depending on the crystallization temperature and the annealing treatment of the ices. Jenniskens and Blake[9] found a crystallization k value of $\sim 5 \times 10^{-4}$ s^{-1} at 150 K for ices grown at 87 K by vapour deposition, and two n values for two different regimes, a first regime with $n = 2$ and a second regime with $n = 0.8$. These parameters agree with those of this work considering the different temperatures of study and the varied histories of the ices.

The recent thorough study of Smith and coworkers[44] is devoted to compact ices grown by vapour deposition with an effusive water vapour beam directed perpendicular to a substrate held at 20 K. Under these conditions the resulting ice samples are assumed to be non-porous. The authors of this work grew ice films of different thickness and studied the crystallization kinetics *via* thermal programmed desorption (TPD) and RAIRS spectroscopy. From the desorption experiments they extracted temperature dependent crystallization rate constants that ranged between 10^{-1} and 10^{-5} s^{-1} in the 170 K–130 K temperature range. They also used the evolution of the OH-stretching band in the RAIRS spectrum of the ice to extract the crystallization rate constant in isothermal experiments conducted at temperatures between 137 K and 149 K. A value of $\sim 1.2 \times 10^{-2}$ s^{-1} was obtained for the crystallization rate constant at 150 K by both techniques. This figure is about two orders of magnitude higher than those found in our work (see Table 1). For the n parameter they found values that range between 2.5 and 5.5, which is attributed to unrestricted three dimensional crystal growth and spatially random nucleation. This is in contrast with our values that range from 1 to 2.4 and point to some constraints either in the nucleation or in the crystal growth geometry. The much higher value of the rate coefficient of Smith *et al.*,[44] which includes both nucleation and crystallization, might have to do with the less restricted nature of the process of nucleation and crystal growth reflected in their higher n parameters.

Summary and conclusions

This article presents a comparative study, based on infrared spectroscopy, of the morphology (bulk compactness) and isothermal crystallization kinetics of amorphous ice produced either by background water vapour deposition (ASW) or by hyperquenching of liquid droplets (HGW). Both ASW and HGW are good candidates for laboratory analogues of astronomical ices under different circumstances, and we are not aware of any previous study of these two ice varieties under comparable experimental conditions.

In accordance with intuitive expectations, ASW deposits are appreciably more porous than their HGW counterparts. Isothermal adsorption experiments conducted at 40 K, using methane as an adsorbing gas, yield surface areas of 280 ± 30 m^2 g^{-1} for the ASW deposits, and of 40 ± 12 m^2 g^{-1} for comparable HGW samples. This factor-of-seven difference is corroborated by the analysis of the intensities of the corresponding OH dangling-bond bands.

The crystallization kinetics was studied at 150 K by following the evolution of the band shape of the OD stretching vibration in ASW and HGW samples with a small amount of HDO. The amorphous deposits were initially formed at 14, 40 and 90 K. An analysis of the measured data, using the Avrami equation, led to comparable rate constants and n parameters for corresponding ASW/HGW pairs, suggesting that the compaction caused by the heating of the ASW sample before crystallization erases a possible influence of its larger initial porosity. Even if the morphologies of HGW and annealed ASW are not identical, the possible differences are not manifested in the crystallization kinetics. However a significant difference was found between the n parameter of the samples generated at 14 K ($n \sim 1$) and that of the rest ($n > 2$) irrespective of the initial bulk morphology. This result supports the possible existence of a structurally different form of amorphous ice for very low generation temperatures, already suggested in previous literature works, although no firm conclusion on this point can be drawn just from our IR data.

Acknowledgements

This research has been carried out with funding from the MCINN of Spain under grant FIS2010-16455. Y. R.-L. acknowledges financial support from CSIC, JAE-Doc Program. We thank Prof. R. Escribano for helpful discussions and M. A. Moreno for technical support.

References

1 T. Bartels-Raush, V. Bergeron, J. H. E. Cartwright and R. Escribano, *et al*., *Rev. Mod. Phys*., 2012, in press.
2 C. G. Salzmann, P. G. Radelli, B. Slater and J. L. Finney, *Phys. Chem. Chem. Phys*., 2011, **13**, 18468.
3 E. F. Burton and W. F. Olivier, *Nature*, 1935, **135**, 505.
4 R. A. Baragiola, Microporous Amorphous Water Ice Thin Films: Properties and their Astronomical Implications, in *Water in confining geometries*, ed. V. Buch and J. P. Devlin, Springer, 2003.
5 R. A. Baragiola, *Planet. Space Sci*., 2003, **51**, 953.
6 A. H. Narten, C. G. Vekatesh and S. A. Rice, *J. Chem. Phys*., 1976, **64**, 1106.
7 P. Jenniskens and D. F. Blake, *Science*, 1994, **265**, 753.
8 P. Jenniskens, D. F. Wilson and M. A. Poborille, *Astrophys. J*., 1995, **455**, 389.
9 P. Jenniskens and D. F. Blake, *Astrophys. J*., 1996, **473**, 1104.
10 A. I. Kolesnikov, J.-C. Li, S. Dong, I. F. Bailey, R. S. Ecclestone, W. Hahn and S. F. Parker, *Phys. Rev. Lett*., 1997, **79**, 1879.
11 N. J. Sack and R. A. Baragiola, *Phys. Rev. B: Condens. Matter Mater. Phys*., 1993, **48**, 9973.
12 W. Hagen, A. G. G. M. Tielens and J. M. Greenberg, *Chem. Phys*., 1981, **56**, 367.
13 A. Hallbrucker, E. Mayer and G. P. Johari, *J. Phys. Chem*., 1989, **93**, 4986.
14 M. A. Zondlo, T. B. Onasch, M. S. Waeshawsky, M. A. Tolbert, G. Mallick, P. Arenz and M. S. Robinson, *J. Phys. Chem. B*, 1997, **101**, 10887.
15 S. LaSpisa, M. Waldheim, J. Lintemoot, T. Thomas, J. Naff and M. Robinson, *J. Geophys. Res*., 2001, **106**, 33351.
16 S. Mitling and K. T. Leung, *J. Phys. Chem*., 2002, **106**, 6234.
17 T. Loerting, K. Winkel and M. Seidl, *et al*., *Phys. Chem. Chem. Phys*., 2011, **13**, 8783.
18 E. Mayer and P. Brüggeller, *Nature*, 1982, **289**, 715.
19 E. Mayer, *J. Phys. Chem*., 1985, **89**, 3474.
20 M. C. Bellissent-Funel, L. Bosio, A. Hallbrucker, E. Meyer and R. Sridi-Dorbez, *J. Chem. Phys*., 1992, **97**, 1282.
21 D. T. Bowron, J. L. Finney and A. Hallbrucker, *et al*., *J. Chem. Phys*., 2006, **125**, 194502.
22 K. P. Stevenson, G. A. Kimmel, Z. Dohnálek, R. S. Smith and B. D. Kay, *Science*, 1999, **283**, 1505.
23 Z. Dohnálek, G. A. Kimmel, P. Ayotte, R. S. Smith and B. D. Kay, *J. Chem. Phys*., 2003, **118**, 364.
24 R. S. Smith, T. Zubkov, Z. Dohnálek and B. D. Kay, *J. Phys. Chem. B*, 2009, **113**, 4000.
25 N. Horimoto, H. S. Kato and M. Kawai, *J. Chem. Phys*., 2002, **116**, 4375.
26 J. Hessinger and R. O. Pohl, *J. Non-Cryst. Solids*, 1996, **208**, 151.
27 M. Eldrup, A. Venhanen, P. J. Schultz and K. G. Lynn, *Phys. Rev. B: Condens. Matter Mater. Phys*., 1985, **32**, 7048.
28 Y. U. Wu, J. Jiang, S. J. Wang, A. Kallis and P. G. Coleman, *Phys. Rev. B: Condens. Matter Mater. Phys*., 2011, **84**, 064123.
29 D. E. Brown, S. M. George, C. Huang, E. K. L. Wong, K. B. Rider, R. S. Smith and B. Kay, *J. Phys. Chem*., 1996, **100**, 4988.
30 M. S. Westley, G. A. Baratta and R. A. Baragiola, *J. Chem. Phys*., 1998, **108**, 8.
31 B. Rowland, M. Fichser and J. P. Devlin, *J. Chem. Phys*., 1991, **95**, 1378.
32 A. Givan, A. Loewenschuss and C. J. Nielsen, *J. Phys. Chem. B*, 1997, **101**, 8696.
33 U. Raut, M. Famá, B. D. Teolis and R. A. Baragiola, *J. Chem. Phys*., 2007, **127**, 204713.
34 A. Bar-Nun, J. Dror, E. Kochavi and D. Laufer, *Phys. Rev. B: Condens. Matter Mater. Phys*., 1987, **35**, 2427.
35 G. A. Kimmel, K. P. Stevenson, Z. Dohnálek, R. S. Smith and B. D. Kay, *J. Chem. Phys*., 2001, **114**, 5284.
36 J. A. Ghormley, *J. Chem. Phys*., 1967, **46**, 1321.
37 E. Mayer and R. Plezer, *Nature*, 1986, **319**, 298.
38 B. Schmitt, J. Ocampo and J. Klinger, *J. Phys*., 1987, **48**, C1-519.
39 C. S. Boxe, B. R. Bodsgard, W. Smythe and M. T. Leu, *J. Colloid Interface Sci*., 2007, **309**, 412.
40 C. Martin, C. Manca and P. Roubin, *Surf. Sci*., 2002, **502–503**, 275.
41 C. Manca, C. Martin and P. Roubin, *Chem. Phys. Lett*., 2002, **364**, 220.
42 C. Manca, C. Martin and P. Roubin, *J. Phys. Chem. B*, 2003, **107**, 8929.
43 L. Schiver-Mazzouli, A. Schiver and A. Hallou, *J. Mol. Struct*., 2000, **554**, 289.
44 R. S. Smith, J. Matthiesen, J. Knox and B. D. Kay, *J. Phys. Chem. A*, 2011, **115**, 5908.
45 W. Hage, A. Hallbrucker, E. Mayer and G. P. Johari, *J. Chem. Phys*., 1994, **100**, 2743.
46 D. J. Safarik and C. B. Mullins, *J. Chem. Phys*., 2004, **121**, 6003.
47 A. Kouchi and T. Yamamoto, *Prog. Cryst. Growth Charact*., 1995, **30**, 83.
48 Y. Oba, N. Miyauchi, H. Hidaka, T. Chigai, N. Watanabe and A. Kouchi, *Astrophys. J*., 2009, **701**, 464.
49 M. Accolla, E. Congiu, F. Dulieu, G. Manico, H. Chaabouni, E. Matar, H. Mokrane, J. L. Lemaire and V. Pirronello, *Phys. Chem. Chem. Phys*., 2011, **13**, 8037.
50 M. E. Palumbo, *Astron. Astrophys*., 2006, **453**, 903.
51 U. Raut, M. Famá, M. J. Loeffler and R. Baragiola, *Astrophys. J*., 2007, **687**, 1070.
52 K. I. Öberg, A. C. Boogert, K. M. Pontoppidan, S. Van den Broek, E. F. van Dishoek, S. Bottinelli, G. A. Blake and N. J. Evans II, *Astrophys. J*., 2011, **740**, 109.
53 B. Maté, O. Gálvez, V. J. Herrero, D. Fernández-Torre, M. A. Moreno and R. Escribano, *Astrophys. J*., 2009, **703**, L178.
54 O. Gálvez, B. Maté, V. J. Herrero and R. Escribano, *Astrophys. J*., 2010, **724**, 539.
55 M. Avrami, *J. Chem. Phys*., 1939, **7**, 1103; M. Avrami, *J. Chem. Phys*., 1940, **8**, 212; M. Avrami, *J. Chem. Phys*., 1941, **9**, 177.
56 B. Maté, A. Medialdea, M. A. Moreno, R. Escribano and V. J. Herrero, *J. Phys. Chem. B*, 2003, **107**, 11098.
57 O. Gálvez, B. Maté, V. J. Herrero and R. Escribano, *Icarus*, 2008, **197**, 599.
58 L. Abad, D. Bermejo, V. J. Herrero, J. Santos and I. Tanarro, *Rev. Sci. Instrum*., 1995, **66**, 3826.
59 R. M. Mastrapa, S. A. Shandford, T. L. Roush, D. P. Cruikshank and C. M. D. Ore, *Astrophys. J*., 2009, **701**, 1347.
60 D. M. Hudgins, S. A. Sandford, L. J. Allamandola and G. G. M. Tielens, *Astrophys. J., Suppl. Ser*., 1993, **86**, 713.
61 M. A. Satorre, M. Domingo and C. Millan, *et al*., *Planet. Space Sci*., 2008, **56**, 1748.
62 V. Buch and J. P. Devlin, *J. Chem. Phys*., 1991, **94**, 4091.
63 J. P. Devlin and V. Buch, *J. Chem. Phys*., 1995, **99**, 16534.
64 B. W. Callen, K. Griffiths and P. R. Norton, *Surf. Sci. Lett*., 1992, **261**, L44.
65 O. Gálvez, B. Maté, V. J. Herrero and R. Escribano, *Astrophys. J*., 2009, **703**, 2101.
66 V. J. Herrero, O. Gálvez, B. Maté and R. Escribano, *Phys. Chem. Chem. Phys*., 2010, **12**, 3164.
67 S. Brunauer, Ph. H. Emmett and E. Teller, Contribution from the Bureau of Chemistry and Soils and George Washington University, Adsorption of Gases in Multimolecular Layers, 1938.
68 N. K. Nair and A. W. Adamson, *J. Phys. Chem*., 1970, **74**, 2229.
69 C. Manca, C. Martin and P. Roubin, *Chem. Phys*., 2004, **300**, 53.
70 W. B. Collier, G. Ritzhaupt and J. P. Devlin, *J. Phys. Chem*., 1984, **88**, 363.
71 N. Uras-Aytemiz, C. Joyce and J. P. Devlin, *J. Chem. Phys*., 2001, **115**, 9835.
72 L. Vrbka and P. Jungwirth, *J. Phys. Chem. B*, 2006, **110**, 18126.
73 M. M. Conde, C. Vega and A. Patrykiejew, *J. Chem. Phys*., 2008, **129**, 014702.

